IAC–19–D2.4.10

A Conceptual Design Study for an Unmanned, Reusable Cargo Lunar Lander

Bradford Robertson[a]*, Eugina Mendez Ramos[b], Manuel J. Diaz[c], Dimitri Mavris[d]

[a] School of Aerospace Engineering, Georgia Institute of Technology, 275 Ferst Dr., United States of America, bradford.robertson@asdl.gatech.edu

[b] School of Aerospace Engineering, Georgia Institute of Technology, 275 Ferst Dr., United States of America, eolivas3@gatech.edu

[c] School of Aerospace Engineering, Georgia Institute of Technology, 100 Exploration Way, United States of America, manueljdiaz@gatech.edu

[d] School of Aerospace Engineering, Georgia Institute of Technology, 275 Ferst Dr., United States of America,

* Corresponding Author

Abstract

Motivated by the aggressive timeline of NASA's Artemis Program, the feasibility of evolving a mid-sized, reusable and refuelable cargo lunar lander technology demonstrator into the descent element of the three-stage human lander was assessed with the goal of forming synergies between both acquisition programs. Requirements for such a concept are that it must be deployed on commercial launch vehicles that are expected to enter into service consistent with Artemis' timeline. In order to assess this concept's feasibility, a physics-based analysis of alternatives was conducted where mission and vehicle architectures are traded side-by-side. Mission trades considered include the impacts of traveling to near-rectilinear halo orbit quickly versus slowly; vehicle trades include fuel and oxidizer tank configurations, number of engines, and propellant combinations, as well as several technology options, e.g. reduced and zero boil-off strategies. Results and discussions are presented to facilitate the consideration of this concept.

Keywords: lunar lander, systems analysis, multidisciplinary design and analysis, space systems, analysis of alternatives,

1. Introduction

Space Policy Directive 1 directed NASA to return "humans to the Moon for long-term exploration and utilization." Vice President Pence has since given NASA a target for a crewed lunar mission by 2024 with "sustainable missions by 2028."As a response to this mandate, NASA initiated the Artemis program. Preliminary plans involve the use of commercial launch vehicles, the construction of the lunar Gateway, and the development of three classes of lunar landers: small, mid-sized, and large.[2,14] NASA categorizes a small lander as one being capable of landing at least 10 kg[1] on the surface of the Moon, mid-sized is considered to be able to land 500 -1,000 kg,[14] and a large lander is capable of crewed missions, landing over 9,000 kg. To date, NASA has already begun acquisition programs for small and large[15] lunar landers.

As part of Artemis' on-going lander acquisition programs, the following key goals and requirements have been outlined: small and mid-sized landers are to land scientific and technology demonstration payloads;[13] mid-sized landers must also demonstrate reusability. The large lander of the Next Space Technologies for Exploration Partnerships -2 (NextSTEP-2) solicitation seeks to refine designs for a three-stage lander where the reference mission architecture involves aggregating all three stages at the Gateway in a Near Rectilinear Halo Orbit (NRHO). Additionally, NextSTEP-2 outlines technology goals of element reusability, cryogenic propulsion, and cryogenic refueling at Gateway.[16] Given the technological complexity of reusable elements, high-energy cryogenic propulsion, and cryogenic fluid management (CFM), a technology demonstrator would reduce the overall risk of the lunar program.

Motivated by Artemis' aggressive timeline, this paper explores the novel concept of how Artemis' descent stage can also be used as a mid-sized reusable cargo lander. This multi-mission lander explores the feasibility of using a single element to fulfill the requirements of both the mid-sized cargo and large crewed lander. This system would be able to take advantage of commercial launch vehicles and refueling opportunities at the lunar Gateway between mis-

sions. The main advantages of such a lander concept are that it can serve as a reusable cargo vehicle that may be able to demonstrate the efficacy of CFM technologies and give the Artemis architecture a path to evolve. Because of the reusable cargo demonstrator, this concept allows for building confidence in the system in order to buy down risk for the crewed missions, as both new technologies and reusability are demonstrated and utilized in the cargo precursor missions.

This study was performed utilizing the Dynamic Rocket EQuation Tool (DYREQT) as the evaluation framework along with a suite of developed modules representing the lander's primary subsystems. DYREQT is a modular, state-of-the-art framework for sizing and synthesis of space systems that enables multidisciplinary design, analysis, and optimization (MDAO) during pre-conceptual and conceptual design.[5,6,18,20,21] The framework, as well as the subsystem models developed for this study, are documented in a related paper.[12] This paper outlines mission parameters, vehicle architectures, and CFM technology trades considered as part of this analysis of alternatives study; sensitivity analyses are also presented. Section 3 covers the ground rules an assumptions of the study, Section 4 details the sizing missions used for this study, Section 5 outlines the tradespace explored as part of this study, Section 6 outlines the technical approach, and Section 7 discusses the results and observations of the study.

2. Descent Stage Requirements

Based on NASA requirements, the required payload of the descent module is at least 9,000 kg with a goal of more than 12,000 kg; therefore this study sizes this mission based on payload masses greater than 9,000 kg with a goal of maximizing landed mass.[16] The anticipated in-space loiter of the descent element is not specified in the NextSTEP-2 Broad Agency Announcement (BAA), but this loiter time can be extensive because the transfer element, descent, and ascent elements must be at Gateway before the crew launches. Therefore, the loiter will be subject to the assumed launch cadence and must be robust to possible crew launch delays.

The sizing missions are subject to several constraints. The first set of constraints is related to launch vehicle compatibility. NASA has outlined two launch vehicle compatibility requirements in the NextSTEP-2 BAA: gross mass at launch and the dynamic envelope. These constraints are listed in Table 1.

Additionally, the lander will need to hover above the lunar surface during descent and be able to throttle down to a thrust-to-weight ratio of less than one for all missions and payloads. As set out in the NextSTEP-2 BAA, this should be done with a 4:1 (goal of 6:1) effective throttle ratio (TR).[16]

Table 1: Launch Vehicles Considered[16]

Constraint	**LV 1**	**LV 2**
Wet Mass at Launch	16,000 kg	15,000 kg
Dynamic Envelope	6.3 m	4.6 m

Because the descent element is launched without a payload, the launch vehicle compatibility constraints are applied to the as-launched configuration. During a crewed mission, the transfer vehicle is responsible for the transfer from Gateway to low lunar orbit (LLO). This leaves the descent element responsible for lunar descent and landing while carrying the mass of the ascent stage.[16]

3. Ground Rules and Assumptions

In order to treat each architecture and its candidate designs as equally as possible, each will be subjected to a common set of ground rules and assumptions as outlined in this section.

3.1 *General*

The basic mass of the vehicle structure is assumed to be 30% of the total vehicle dry mass (refer to Section 6.1.3 for details). In this 30%, all primary and secondary structures, including the landing gear, are accounted for.

3.2 *Reserves and Margins*

Each vehicle will have a 2.5% flight performance reserve applied to each burn. An additional 1% was added to main propulsion system (MPS) propellants for additional reserves. A mass growth allowance of 25% was applied in addition to the vehicle's dry mass to determine the inert mass used for ΔV calculations.

3.3 *Main Propulsion System*

The cryogenic propellants are assumed to be powered by expander cycles. Each propellant's I_{sp} and oxidizer-fuel ratio (OFR) are assumed to be constant. The I_{sp} and OFR ratio of each propellant combination is shown in Table 2.

Both cryogenic propellant options are pressurized by gaseous helium; both storable options are pressurized by supercritical liquid helium similar to the Apollo lunar descent module.

The mass of a LOX/LCH_4 engine was assumed to weigh 90% of a LOX/LH_2 engine to account for the

Table 2: Assumed MPS Performance

Propellant	**I_{sp}**	**OFR**
LOX/LCH_4	360s	3.5
LOX/LH_2	450s	6.0
NTO/MMH (Pump-fed)	335s	1.9
NTO/MMH (Pressure-fed)	320s	1.75

smaller turbopump assembly; NTO/MMH pressure-fed engine mass is 80% of LOX/LH_2 design, whereas the pump-fed is also assumed to be 90% of LOX/LH_2 engine.

It is also assumed that the time in which the engines are used is small compared to the overall mission duration, hence the heat radiated from the engine(s) onto the vehicle, as well as any other ΔV losses that are not discussed in Section 4, are considered to be negligible. It is assumed that the propellant and I_{sp} penalties for engine start-up and shutdown are also negligible.

Table 3: Assumed Minimum Throttle Capabilities

Propellant	**TR_{min}**
LOX/LCH_4	65%
LOX/LH_2	12%
NTO/MMH (Pump-fed)	12%
NTO/MMH (Pressure-fed)	10%

3.4 *Reaction Control System*

The reaction control system (RCS) of the lander is assumed to be a pressure-fed NTO/MMH system with an I_{sp} of 300s. The RCS is comprised of four pods, each with four 100 lb_f thrusters. Propellant settling maneuvers are assumed to be performed by the RCS through ullage burns.

3.5 *Power System*

The power subsystem is comprised of photovoltaics to generate power with rechargeable Li-Ion batteries that serve as on-board supplemental power storage. The photovolatic system is assumed to have a transmission efficiency of 90%, cell efficiencies of 17.5%, a degradation rate of 3.75%/yr, and an array density of $5kg/m^2$. The batteries are assumed to have a maximum depth of discharge of 50% and a specific storage capacity of 150 W-h/kg. The margin on the power draw required from the photovoltaics is 1,000 W, whereas the battery storage system has a margin of 3,000 W. The photovoltaic system is sized to the industry standard practice of end-of-life at maximum distance operations after degradation is taken into account. Similarly, the batteries are sized to one battery bank; an additional, identical, battery bank was included for redundancy.

3.6 *Avionics*

Each architecture carries an avionics suite consisting of three reaction wheels and six control moment gyros. The sensing equipment suite aboard includes three gyros, three sun sensors, three star sensors, a horizon sensor, a magnetometer, and terrain and hazard navigation. Lastly, the descent module carries deep space communication antennae and related equipment. This suite requires 184 kg of avionics equipment, and has a power draw of 946.6W, of which 90% was assumed to be rejected in the form of heat, i.e. 851.9 W of heat. An additional 4% was assumed to constitute cable mass.

3.7 *Tank Configurations*

Each MPS tank is composed of Al 2195. All pump-fed engine options require the fuel tanks to be pressurized at 30 psia; oxidizer tanks are pressurized at 40 psia. All pressure-fed engine options require a tank pressurization of 250 psia in both the oxidizer and fuel tank. The tanks are sized to be a constant thickness as a function of the ullage pressure with a safety factor of 1.5. Additionally, each tank is sized to accommodate 5% ullage.

The RCS is assumed to be powered by two pairs of spherical tanks. These tanks are sized to an ullage pressure of 250 psia based on the material strength of AL 2195 with a safety factor of 1.5.

3.8 *CFM*

Each propellant tank utilizes 30 layers of Variable Density Multi-Layer Insulation (MLI), with 6, 9, and 15 layers in the inner, middle, and outer segments, and corresponding densities of 8, 12, and 16 layers/cm. In addition, spray on foam insulation (SOFI) with a thickness of 25 mm and a density of 36.8 kg/m^3 is utilized for tanks with cryogenic propellants; while its contribution to thermal mitigation in in-space environments is small, it is included for its effectiveness during ground and launch operations.[7] Tanks that contain storable propellants are, in addition to 30 layers of MLI, covered with a heating element.

The temperature of the surrounding tank support structure and penetrations is determined by the propellant combination used. It is assumed that the temperature of the support structure and penetrations for the colder propellant is set to two-thirds of the

storage temperature of the warmer propellant. The temperature of the structure and penetrations for the warmer propellant is set to the storage temperature of that propellant.

In an attempt to mitigate the mass penalty incurred by incorporating cryocoolers, a single cryocooler is used to remove the combined heat load from two tanks and is sized based on the amount of cooling required - either reduced boiloff (RBO) or zero boiloff (ZBO). In the event an odd number of tanks exist, a single cryocooler is dedicated to each tank. Further, cryocoolers are not shared across tanks of different propellant types. For example, the five tank configuration - a single fuel tank surrounded by four oxidizer tanks - would consist of three cryocoolers: one for the fuel tank and one for each pair of oxidizer tanks.

3.9 *Thermal Environment*

The thermal environment of the lunar surface was used when modeling the thermal control subsystem, as it was the most thermally constraining portion of the mission. Other assumed values include: 207 K for the surface temperature, 0.12 for the surface albedo, and zero for the beta angle (the angle between the solar vector and the local zenith vector with the minimum occurring at local noon).

3.10 *Operation During Eclipse*

Batteries are the sole source of power during operations in eclipse. The primary power draw on the spacecraft comes from the cryocoolers, if used. However, while the spacecraft is in shadow, the thermal environement is much less constraining than when operating in sunlight. It is assumed that, during this time, the cryocoolers do not need to provide the same amount of heat removal and can run at reduced power. Thus, during eclipse operations, the batteries are sized to provide power to the entire spacecraft, albeit reduced from the power required in sunlight operations, plus an additional margin.

4. Missions and ΔV Budget

The lunar lander was sized to perform two missions – a reusable mid-sized cargo lander mission and the Artemis crewed landing mission – to define a multi-point design. The cargo mission is composed of two main phases: the Deployment and Reuse mission phases. A bat chart depicting the reusable cargo lander is shown in Figure 1a; a bat chart depicting the the Artemis crewed landing mission is shown in Figure 1. This study trades four payloads: a deployment mission payload, m_{pl_1}, a reuse payload, m_{pl_2}, a payload that is returned to Gateway, m_{pl_3}, and the Artemis crewed landing payload, m_{pl_4}. Additionally, the lunar lander stays on the surface for a duration of Δt_1 in the Deployment mission phase of the cargo mission; in the Reuse mission phase of the cargo mission, it stays on the surface for a duration Δt_2. For the Artemis crewed landing mission, a duration of Δt_3 is assumed between the descent stage being staged at Gateway and it performing the descent from LLO. These variables represent mission-level trades where the payloads can be traded against different lander designs. This results in a constrained multi-objective design space where the different payloads drive the size of the lander.

For all sizing missions, the ΔV required for lunar ascent and descent are parametric functions of vehicle properties to account for gravity losses. For this study, ΔV curves were regressed based on data derived from Altair design studies.[10,11] The lunar descent relationship, shown in Equation 1a and Figure 2, is based solely on the thrust-to-Earth-weight ratio at the beginning of descent; the constant represents the ideal ΔV needed to descend and the other term accounts for ΔV losses due to gravity. The lunar ascent relationship, shown in Equation 1b and Figure 2, is based on both the Earth thrust-to-weight at liftoff and the I_{sp} of the MPS; the constant represents the ideal ΔV needed to ascend and the two other terms account for ΔV losses due to gravity.

$$\Delta V_{descent} = 1911.67 + 1.92 \left[\frac{T}{W_0}\right]^{-2.82} \tag{1a}$$

$$\Delta V_{ascent} = 1698.87 + 0.10 I_{sp} + 1.33 \left[\frac{T}{W_0}\right]^{-3.33} \tag{1b}$$

4.1 *Cargo Mission*

The cargo mission represents the use of an Artemis descent element as a mid-sized lunar lander that is capable of serving as a technology demonstrator to advance reusability, CFM, and refuelability. In order to demonstrate these technologies, the cargo mission is comprised of two major phases: the Deployment and Reuse mission phases. The Deployment mission phase is the lander's primary mission phase where a payload is deployed on the lunar surface. The secondary phase, the Reuse mission phase, is where reusability and refueling are demonstrated by performing at least two round-trips to Gateway, while delivering payloads from Gateway to the surface and vice versa.

The descent stage's Deployment mission phase begins after it is inserted into a trans-lunar injection

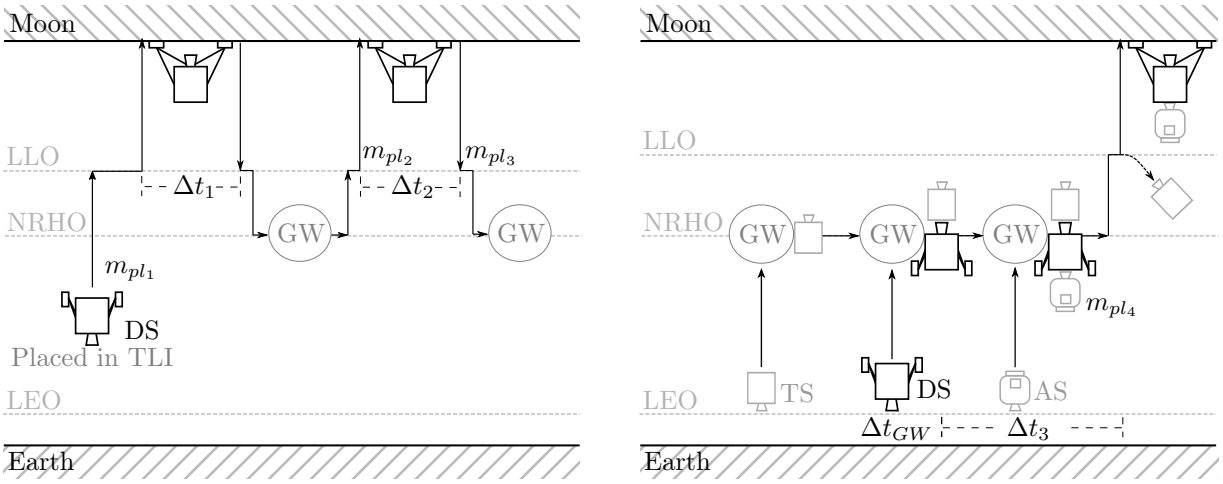

(a) Cargo and Reuse

(b) Crewed

Fig. 1: CONOPS Bat Charts

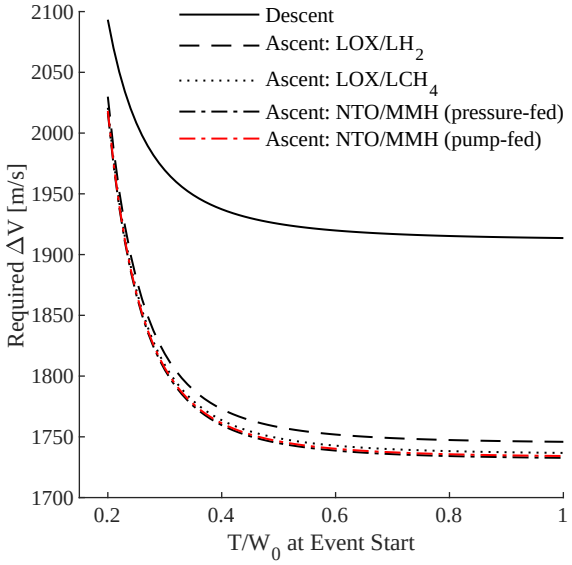

Fig. 2: Delta-V Curves

(TLI). It is assumed that the Earth-Moon transit time is 4.1 days and the lander stays in LLO for 0.5 days before it descends. The descent is modeled in two segments: the initial descent from LLO, which is modeled via Equation 1a, and the terminal descent segments. Terminal descent is assumed to require 50 m/s, allowing the descent stage to hover for hazard avoidance until soft touchdown occurs. After touching down, the deployment payload (m_{pl_1}) is unloaded and stays on the surface for a duration of Δt_1 days. The complete definition of the Deployment mission phase is shown in Table 4.

The Reuse mission phase begins when the lander ascends back to Gateway with no payload onboard. Once it docks with Gateway, the lander's MPS and RCS propellants are refueled, and it is given a reuse payload (m_{pl_2}), as shown in Figure 1a. Afterwards, it undocks from Gateway and descends from NRHO to LLO and down to the surface where it stays for a duration of Δt_2 and offloads the reuse payload brought from Gateway. Unlike the Deployment mission phase, the Reuse mission phase also has the option of returning to Gateway with a return payload, m_{pl_3}. Regardless of whether the lander had a return payload or not, it ascends again and docks with Gateway.

4.2 *Artemis Mission*

The preliminary Artemis crewed landing mission architecture consists of three stages that will aggregate at Gateway; a representative concept of operations is depicted in Figure 1. The descent element is inserted into TLI. From there, it can insert itself into NRHO to dock at Gateway via a fast transit or a slow ballistic lunar transfer. This choice represents a mission tradeoff – the fast transit consists of a transit duration of three days and requires 450 m/s to perform the NRHO insertion burn; the slow transit consists of a transit duration of 120 days and a 30 m/s NRHO insertion burn.[3] The ΔV budget for this mission and corresponding propulsion systems can be seen in Table 5; the fast or slow Gateway transit options are represented via the ΔV_{GW} (Equation 2a) and Δt_{GW} (Equation 2b) variables.

Table 4: Descent Stage's Portion of Cargo Mission

	Event	Propulsion System	Metric
Deployment Phase	TCM 1	RCS	20 m/s
	Lunar Transit		2 days
	Mid-course TCM 2	RCS	5 m/s
	Lunar Transit		2.1 days
	TCM 3	RCS	5 m/s
	LOI	MPS	880 m/s
	LLO TCM	RCS	10 m/s
	Loiter		0.5 d
	Descent RCS 1	RCS	15 m/s
	Lunar Descent	MPS	Eqn. 1a
	Descent RCS 2	RCS	10 m/s
	Terminal Descent	MPS	50 m/s
	Detach Deploy. P/L		$-\Delta m_{pl_1}$kg
	Surface Stay		Δt_1 days
Reuse Phase	Takeoff	MPS	50 m/s
	Ascent RCS 1	RCS	10 m/s
	Ascent	MPS	Eqn. 1b
	Ascent RCS 2	RCS	5 m/s
	NRHO Transfer	MPS	646 m/s
	TCM 4	RCS	10 m/s
	NRHO Transfer		0.5 days
	NRHO Insertion	MPS	84 m/s
	Docking RCS	RCS	5 m/s
	Dock at Gateway		
	Attach Reuse P/L		$+\Delta m_{pl_2}$kg
	Top-off Propellants	MPS&RCS	
	Undock from Gateway		
	LLO Transfer Burn	MPS	84 m/s
	TCM 1 to LLO	RCS	10 m/s
	Transfer Duration		0.5 days
	LOI Burn	MPS	646 m/s
	LLO TCM	RCS	20 m/s
	Descent RCS 1	RCS	15 m/s
	Lunar Descent	MPS	Eqn. 1a
	Descent RCS 2	RCS	10 m/s
	Vertical Drop	MPS	50 m/s
	Surface Stay		Δt_2 days
	Detach Reuse P/L		$-\Delta m_{pl_2}$kg
	Attach Return P/L		$+\Delta m_{pl_3}$kg
	Takeoff	MPS	50 m/s
	Ascent RCS 1	RCS	10 m/s
	Ascent	MPS	Eqn. 1b
	Ascent RCS 2	RCS	5 m/s
	NRHO Transfer	MPS	646 m/s
	NRHO Transfer TCM	RCS	10 m/s
	NRHO Insertion	MPS	84 m/s
	Docking RCS	RCS	5 m/s
	Dock at Gateway		

Table 5: Descent Stage's Portion of Artemis Crewed Landing Mission

Event	Propulsion System	Metric
Transit to NRHO	MPS	Δt_{GW} days
NRHO Insertion	MPS	ΔV_{GW} m/s
NRHO TCM	RCS	20 m/s
Stay at Gateway		Δt_3 days
Attach Ascent Stage		$+m_{pl_4}$ kg
Undock from Gateway		
Transit to LLO		0.5 days
Descent RCS 1	RCS	15 m/s
Lunar Descent	MPS	Eqn. 1a
Descent RCS 2	RCS	10 m/s
Terminal Descent	MPS	50 m/s

$$\Delta V_{GW} = \begin{cases} 450 \text{ m/s} & \text{if GW transit = fast} \\ 30 \text{ m/s} & \text{if GW transit = slow} \end{cases} \quad (2a)$$

$$\Delta t_{GW} = \begin{cases} 3 \text{ days} & \text{if GW transit = fast} \\ 120 \text{ days} & \text{if GW transit = slow} \end{cases} \quad (2b)$$

In addition to the Gateway transfer option, this mission has two additional degrees of freedom: the time elapsed between the lander docking at Gateway and its portion of the mission and the total mass of the ascent stage. These degrees of freedom are represented via the Δt_3 and m_{pl_4} variables, respectively. The total mass of the ascent stage is assumed to include the crew and all necessary equipment to sustain them.

5. Vehicle Architecture Tradespace

In order to assess the feasibility of this concept, several architectural alternatives were considered. Each architecture is defined as a unique combination of the following with regard to the MPS: propellant type, propellant feed system, number of engines, number of fuel and oxidizer tanks, and CFM approach. Within each category, a limited number of architecture alternatives were considered: LOX/LH_2, LOX/LCH_4, and NTO/MMH MPS propellant types; pressure and pump-fed propellant feed architectures; one or three engines; two fuel and two oxidizer or one fuel and four oxidizer tanks; and passive, reduced boil-off, or zero boil-off CFM technologies. Table 6 shows a matrix of alternatives that summarizes this tradespace. In total, there are 72 architecture alternatives to evaluate and trade. However, some incompatibilities among the options exist:

- NTO/MMH is not cryogenic, and thus is incompatible with any active CFM system
- The active RBO CFM approach is not applicable to LOX/LCH$_4$
- Pressure-fed LOX/LH$_2$ and LOX/LCH$_4$ architectures were not considered

Removing these incompatible combinations results in 28 vehicle architecture alternatives to assess.

Table 6: Vehicle Architecture Matrix of Alternatives

MPS	LOX/LH$_2$	LOX/LCH$_4$	NTO/MMH
Propellant Feed	Pump	Pressure	
Engines	1	3	
MPS Fuel&Ox Tanks	2&2	1&4	
CFM	Passive	RBO	ZBO

5.1 *Main Propulsion System*

The engine configurations assumed are either one engine or three engines. The only assumed configuration of three engines is in-line, as shown in Figure 3. The reason for only considering the in-line engine configuration was driven by the hover requirement, which may require turning off the engines in order to stay above the assumed minimum throttle ratios (TR) shown in Table 3; each engine's maximum TR is assumed to be 100% of the specified thrust level. In the case of a three engine architecture, one or two engines may be turned off to prevent deep throttling of all engines. Engine-off hover and landings are only assumed if the TR required to hover is lower than its corresponding value in Table 3. When that occurs, the TR required for a single engine shut-down (i.e. the center engine) is calculated, with the powered hover and descent performed via the outboard engines. If the TR required is lower than the minimum TR, then two engines are shut-down (i.e. the two outboard engines), and the powered hover and descent is performed via the center engine only. If that TR required is still lower than the minimum TR, then the candidate design is considered to be infeasible.

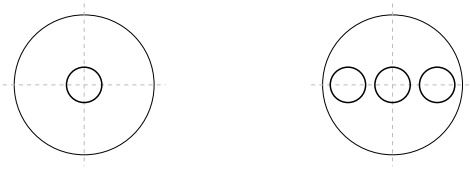

(a) 1 Engine (b) 3 Engines

Fig. 3: Engine Configurations Considered

5.2 *MPS Tank Configurations*

The number of MPS tanks considered are two fuel and two oxidizer tanks, and one fuel and four oxidizer tanks. Figure 4 illustrates how these tanks are configured. Through this configuration, the stage's diameter is calculated via Equation 3.

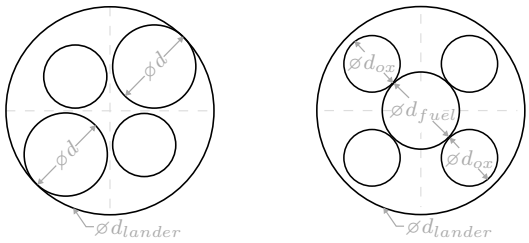

(a) 2 Fuel & 2 Ox (b) 1 Fuel & 4 Ox

Fig. 4: Top View of Tank Configurations Traded

$$d_{lander} = \begin{cases} 2 \times 1.2 \max(d_{fuel}, d_{ox}) & \text{if } \mathrm{n_{tanks}} = 4 \\ 1.2(d_{fuel} + 2d_{ox}) & \text{if } \mathrm{n_{tanks}} = 5 \end{cases} \quad (3)$$

Additionally, the dimension of the fuel and oxidizer tanks are traded via the length over diameter (L/D) ratio. An L/D=1 translates to a spherical tank and an L/D>1 is defined as two hemispherical domes connected via a cylindrical barrel section. To illustrate the L/D parameter, Figure 5 shows three tanks side-by-side, each with different L/D values. All tanks in this figure contain equal volumes.

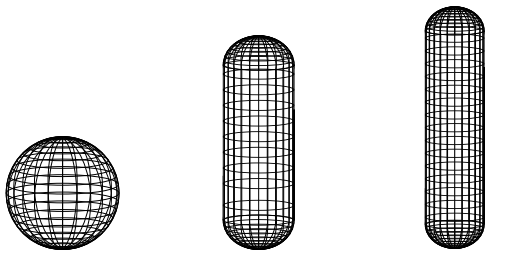

(a) L/D = 1 (b) L/D = 3 (c) L/D = 5

Fig. 5: Examples of Equal Volume Tanks

5.3 *CFM*

The final system being traded is the CFM system for the cryogenic propellants LOX/LH$_2$ and LOX/LCH$_4$. Passive and active options are available; the system configuration depends on the propellant combination utilized and the amount of boil-off reduction desired.

MLI and SOFI constitute the passive CFM system and can be used exclusively but will result in higher boil-off loses than if an active system were used. In addition to MLI, the lander can utilize active CFM in order to further reduce boil-off losses. Landers incoporating LOX/LCH_4 can utilize a Zero Boi-Off (ZBO) configuration consisting of 90 K cryocoolers. Landers utilizing LOX/LH_2 have the option incorporating a ZBO configuration consisting of 20 K cryocooler(s) for LH_2, and 90 K cryocooler(s) for LOX. These landers also have the option for a Reduced Boil-Off (RBO) configuration which uses 90 K cryocoolers for both propellants and incorporates a vapor-cooled/broad area cooling (BAC) shield to reduce boiloff of LH_2.[17]

6. Technical Approach

The technical approach taken to design a lander capable of performing both the mid-sized reusable cargo and human landing missions outlined in Section 4 is discussed in this section. With the mission and vehicle architecture tradespaces defined, all architecture combinations are enumerated, resulting in 56 architectures to trade. Due to the numerous architecture options, it is necessary to define, characterize, and search the vehicle's design space.

Each architecture's design space, shown in Table 7, is defined via nine degrees of freedom, each with minimum and maximum bounds. The total thrust is defined as the summed thrust of all MPS engines at 100% TR; the fuel and oxidizer tanks' length-to-diameter (L/D) ratios trade the basic geometry of the tanks; the deployment, reuse, returned, and ascent element payload masses trade different performance requirements on the vehicle; and the deployment, reuse, and Gateway durations trade mission requirements and their impact on the vehicle's performance. For simplicity, the deployment and reuse surface stay durations were assumed to be equal.

Table 7: Vehicle and Mission Design Space

Variable	**Min**	**Max**	**Units**
Total Thrust	35	150	kN
Fuel Tank L/D Ratio	1	5.0	–
Ox. Tank L/D Ratio	1	5.0	–
Deploy. Payload, m_{pl_1}	1	1,750	kg
Reuse Payload, m_{pl_2}	1	3,500	kg
Returned Payload, m_{pl_3}	1	3,500	kg
Ascent Element, m_{pl_4}	9,000	15,000	kg
Surf. Stays, $\Delta t_1 = \Delta t_2$	7	30	days
Stay at Gateway, Δt_3	30	120	days

To fully define each architecture's design space, it is necessary to evaluate numerous candidate designs. In order to evaluate each architecture's design space efficiently, the sampling technique of design of experiments (DoEs) was utilized; approximately 10,000 candidate cases per architecture were evaluated. Because of the diverse number of architectures and numerous candidate designs that need to be evaluated, a suitable evaluation framework is necessary. The criteria for a suitable framework are it must be physics-based, it must synthesize the disciplines that constitute a lunar lander, it must size the disciplines such that it must be capable of performing its missions, it must be automated, and that it is inexpensive to run. In order to fill this need, the DYnamic Rocket EQuation Tool (DYREQT),[5,6,18,20,21] a recently-developed sizing and synthesis framework built upon OpenMDAO[8,9] for the pre-conceptual and conceptual design of space systems, was utilized. One of the key features of DYREQT is that it leverages external codes representing disciplines that constitute space systems, e.g. tanks, engines, etc. and uses them to dynamically assemble the corresponding MDAO problem in order to size and synthesize the specified architecture. As such, a suite of modules that represent the various disciplines that must be sized and synthesized in order to define a lunar lander concept was developed;[12] a brief overview of each is presented in the sections below. DYREQT is written in Python 3, as are most of the external modules, though some call pre-compiled FORTRAN 90 executables.

Evaluating each case takes approximately six seconds for each Passive CFM case and 15 seconds for each ZBO CFM case. All 560,000 cases are typically evaluated in 48hrs on a single, modern workstation capable of running 35 parallel processes. When cluster resources are utilized, this wall-time is significantly reduced.

In order to evaluate the tradespace, neural networks for each architecture were trained in JMP Pro version 14. These neural networks featured two layers of 45 fully-connected nodes and were trained utilizing k-fold cross-validation. Neural networks were used in place of more traditional response surface equations because of the complexity of the design space. For example, at any given point in the design space, one of the four payloads drives vehicle sizing while the other three payloads have essentially no effect on vehicle size; the neural network is able to accurately capture this behavior and enables fast design space exploration.

6.1 *Contributing Analyses*

This section briefly discusses each of the modules used to size the lander's primary subystem. These include the power, avionics, structures, engines, tanks, and thermal control subystems. Each model returns the basic mass of the subsystem, the power required, and the heat load generated (if applicable). For a more detailed discussion regarding the model inputs, outputs, and sizing methods used, the reader is referred to the related work, *Development of a Physics-Based Reusable Cargo Lunar Lander Modeling and Simulation Capability.*[12]

6.1.1 *Power*

The power subsystem consists of three primary components - the power generator, energy storage, and regulation/distribution. The model receives the power requirements from each of the subsystem models (where applicable) as an input and sizes the solar arrays to satisfy the total power requirement for the spacecraft. The model also receives the amount of supplemental power required as an input; batteries are sized based on this requirement, and the mass of the regulation/distribution is based on a percentage of the cumulative mass of the solar arrays and batteries. The heat load generated by the fuel cells is a function of fuel cell efficiency, and the heat load from the batteries is estimated to be 10% of the battery power.

6.1.2 *Avionics*

The avionics subsystem mass is the sum of the masses of the sensors, actuators, and a communications package. These masses are estimated based on data from flight certified commercially available hardware.[22] The masses of the sensors and actuators scale with the vehicle mass, while the mass of the communications package scales with the distance from Earth. The total power requirement for the subsystem is the sum of the power required by each category of component - sensors, actuators, and communications package. The heat load generated by the subsystem is estimated to be 90% of the total power requirement.

6.1.3 *Structures*

The structure mass is based on the published structure mass percentages of several historical and conceptual space systems, e.g. Mercury, Gemini, Apollo, and other conceptual studies. A least square regression applied to the above vehicles yielded a structure mass percentage of 28%, with an R^2 value of 0.966. Based on this value, a conservative value of 30% was used to estimate the lander structure mass.

6.1.4 *Engines*

The engines subsystem mass consists of the engine(s), propellant management hardware associated with the physical engine(s), and miscellaneous hardware associated with plumbing. The engine mass scales with thrust, the mass of the propellant management hardware is 10% of the engine mass, and the mass of miscellaneous hardware is 15% of the combined mass of the propellant management hardware and the engine(s).

6.1.5 *Tanks*

The tanks subsystem model sizes propellant storage devices for the MPS and RCS systems. The subsystem mass consists of the tank, a liquid acquisition device (LAD), hardware such as plumbing, brackets and insulation, trapped propellant, and pressurant. The LAD and hardware masses are estimated to be 53.7% and 15% of the tank mass, respectively. The mass of the trapped propellant is 1% of the useable propellant mass, and the pressurant is sized to fully expel the propellant from the tank.

6.1.6 *Thermal Control*

This model provides sizing of thermal control systems for propellant and pressurant tanks, and the spacecraft. Sizing occurs in three parts: passive cooling, active cooling, and heat rejection. Passive and active sizing of CFM systems occurs via NASA's Cryogen Storage Integrated Model, or CryoSIM.[19]

The Passive CFM mass consists of the mass of the MLI, SOFI, and propellant mass gauge. The mass of the MLI is determined from the number of layers used in each of the inner, middle, and outer segments, and the corresponding density of each of these segments; the mass of the SOFI is based on its density and thickness. Both the MLI and SOFI mass scale with the surface area of the tank. The mass and power requirement of the mass gauge scale with the longest dimension of the tank.

The active CFM system mass includes the mass of the crycoolers and the BAC shields; components requiring power include the cryocooler and circulator. The mass and power required for these components is estimated using scaling equations in CryoSIM (see *Mendez-Ramos, et al.*[12] for further details).

The final component sized by the thermal subsystem model is the spacecraft radiator which is used to reject excess heat to the environment. The heat load from the subsystem models, including the heat intercepted by the cryocoolers, is used to estimate the

radiator mass.

7. Results and Observations

The first step in analyzing the design space is to examine the tradeoffs between different MPS and CFM system combinations. In order to do this, the neural nets trained in Section 6 were run through a Non-Dominated Sorting Genetic Algorithm II (NSGA-II)[4] in order to find the best-of-breed architectures for each combination. The NSGA-II is optimizing to find the Pareto Frontier between the Artemis crewed landing mission payload and the unmanned cargo mission deployment payload; these two payloads drive the overall sizing of the lander. The Pareto Frontier represents a family of feasible designs that the designer can use to make informed trades, i.e. moving along the line means improving one metric while compromising the other. Since each launch vehicle carries unique constraints, this analysis was repeated for each launch vehicle in order to assess the impacts of choosing either one. The results of this analysis can be seen in Figure 6; each MPS/CFM combination that is able to perform the sizing mission is shown.

From results in Figure 6, several general observations can be made: most architectures have a unique "knee" in the curve. This knee is due to, as m_{pl_1} increases, it starts to drive the design and vice versa. Additionally, with the exception of passive LOX/LH_2, all best-of-breed architectures utilize a single engine, four MPS tanks, and a ballistic transfer to Gateway; the LOX/LH_2 RBO architecture that utilizes a fast transfer to Gateway (purple line) is dominated by the same architecture utilizing a slow transfer to Gateway (blue line). Passive LOX/LH_2 utilizes the five tank configuration and a fast Gateway transfer because it significantly reduces boil-off. Specifically for LV1 (Figure 6a), several observations can be made:

1. Pump-fed NTO/MMH (red line) provides excellent performance, exceeding the payload requirements outlined in NextSTEP-2.
2. At minimum mission durations and a fast transit to Gateway, LOX/LH_2 Passive (green line) also exceeds NextSTEP-2's payload requirements.
3. No designs of the ZBO LCH_4 architecture (yellow line) meet NextSTEP-2's payload requirements.
4. At minimum mission durations while transferring to Gateway with the slow option, RBO LOX/LH_2 is the highest performing architecture.
5. No designs of Pressure-fed NTO/MMH, Passive LOX/LCH_4, nor ZBO LOX/LH_2 closes, i.e. those architectures are infeasible.

Similarly, several observations can be made for LV2 (Figure 6b):

1. LCH_4 architectures are infeasible.
2. Pump-fed NTO/MMH, as well as, Passive and RBO LH_2 architectures are feasible among both LVs, albeit with slightly reduced performances on LV2.

A final observation that can be made from Figure is that best MPS–CFM combinations are pump-fed NTO/MMH and RBO LOX/LH_2. However, RBO LOX/LH_2 represents a technology that might not be achievable for a 2024 flight, but because passive LOX/LH_2 is feasible, a possible evolutionary path exists.

7.1 *Evolutionary Path to RBO LOX/LH_2*

The first step at examining an evolutionary path is determining the architecture of a LOX/LH_2 lander. Figure 8 shows a comparison between four and five tank configurations with a single engine, a 9,000 kg crewed landing payload for different in-space loiters at Gateway; the designs used for this plot utilize a minimum deployment cargo payload to assess the feasibility of passive systems for use with the Artemis crewed mission. For the passive case, the five tank lander dominates the four tank lander; for the RBO case, the four tank lander dominates the five tank lander, Because both passive architectures are feasible for the Artemis human landing mission, a path forward for evolving a LOX/LH_2 lander exists. The key tradeoff is the anticipated robustness of a passive LOX/LH_2 lander to in-space loiter at Gateway versus the eventual capability of an RBO lander.

Figure 7 shows the sensitivity of both the four and five tank, passive LOX/LH_2 landers to in-space loiter both for the Artemis crewed mission and reusable cargo missions; each architecture is sized based on a single engine, a 9,000 kg crewed landing payload and a 500 kg deployment cargo payload. One note on this figure is that the vehicles are only sized to the crewed landing mission– the four tank lander does not close with a 500 kg deployment cargo payload while simultaneously being sized to a 9000 kg crewed landing payload. However, the four tank lander is very close to closing for both missions; possible technology infusions (such as an externally deployable sun shade) that would improve a passive CFM system's performance not addressed in this study that could reduce

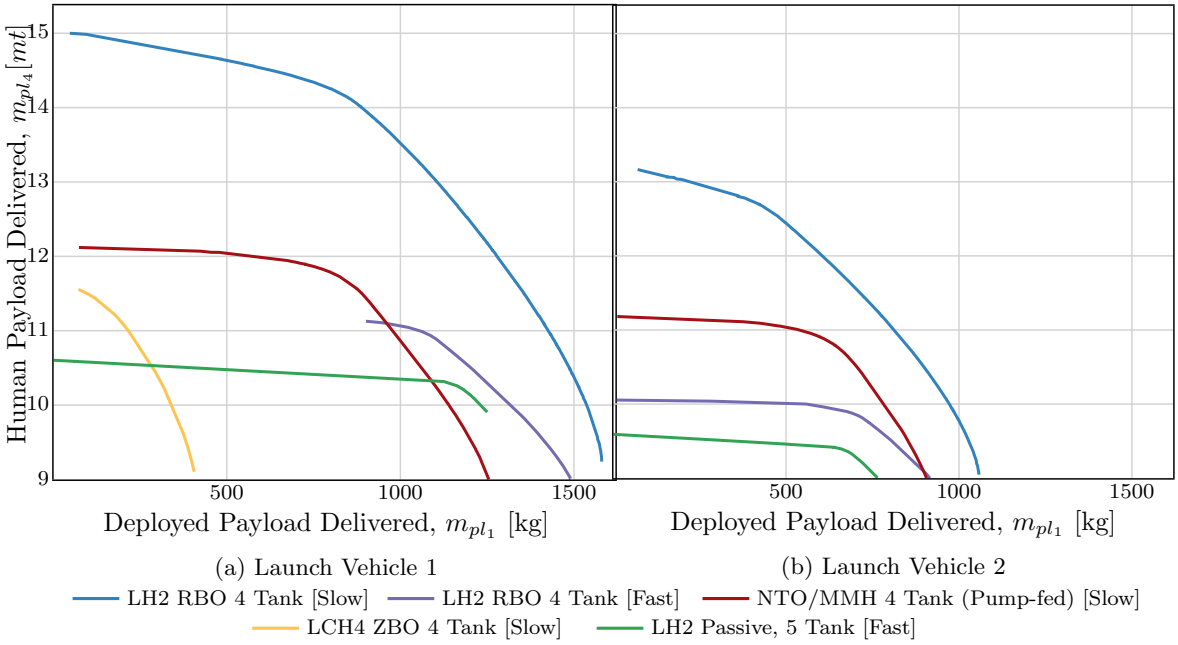

Fig. 6: Constrained, Pareto Frontiers showing best of breed architectures for minimum mission durations for non-dominated MPS–CFM combinations. Each architecture has 1 Engine.

boiloff during the in-space loiter at Gateway and push the four tank lander into feasibility.

7.2 *Use of Existing Engines*

Another consideration in the tradespace is that the 2024 mission will likely require the use of existing engines. Figure 9 shows the Pareto Frontiers of the LOX/LH_2 systems and pump-fed NTO/MMH systems with existing engines. The first row compares the human payload, m_{pl_4}, delivered vs. the deployed payload delivered,m_{pl_1}, for both launch vehicles with minimum reuse (m_{pl_2}) and recycle payloadsm_{pl_3}; the second row compares the reuse payload, m_{pl_2}, delivered vs. the deployed payload delivered,m_{pl_1}, for both launch vehicles for a fixed human payload of 9,000kg. All mission durations were held at minimum values, i.e. $\Delta t_1 = \Delta t_2 = 7$days and $\Delta t_3 = 30$days, however, the Gateway transit option was traded. The LOX/LH_2 configurations use a single RL10C-1 engine with 102 kN; the NTO/MMH configuration uses a single RS-72 engine with 55.4 kN of thrust. From this figure, several key takeaways can be gleaned:

1. The architecture and engine selection is subjected to a value proposition: the crewed missions on either launch vehicle perform best with LH_2 RBO 4 tanks with the Slow Gateway transit option and for reuse cargo mission, NTO/MMH is the best performing. For missions that compromise between human and deployment payloads, the optional architecture and engine selection depends on the degree of compromise.
2. For cargo mission, both NTO/MMH and LH_2 RBO 4 tank options were able to deliver the maximum reuse payload considered of 3,500kg for LV1; LV2 is also able to deliver over 3,300kg of reuse payload at the cost of no deployment payload delivered.
3. both LH_2 RBO and NTO/MMH with 4 tanks perform well across both LVs and both sets of cargo and human missions.
4. The LOX/LH_2 RBO 4 and NTO/MMH architectures can perform a cargo-heavy mission in addition to landing 9,000kg of m_{pl_4} payload; LOX/LH_2 Passive cannot.

In the case of the human mission, however, is that none of these engines are man-rated, therefore, a man-rating effort would need to be taken in order to perform the human missions.

Another dimension of this tradespace concerns the cargo landing missions. Figures 9c and 9d show2 the relative reuse mission capability for the LOX/LH_2 and pump-fed NTO/MMH landers. From these two plots, it is clear that the NTO/MMH system outperforms the LOX/LH_2 systems ; this occurs because

of the additional mass incurred by the RBO CFM system. This represents another value proposition: LOX/LH_2 systems can provide more performance for the crewed mission while NTO/MMH systems provide more performance for cargo missions.

8. Conclusion

This paper presents an analysis of alternatives for multi-mission lunar landers utilizing a novel approach with modern MDAO tools. Several contributing analyses were synthesized in order to size disparate architectures of lunar landers as a function of vehicle design parameters, payloads, and mission options. Artificial neural networks and multi-objective optimization algorithms were used to explore the trade space to determine best-of-breed architectures for multiple missions.

The results of this analysis show that the descent stage of the Artemis crewed landing system can be used as a stand-alone reusable cargo lander. Based on the analysis of alternatives, the noted assumptions of the study, and the underlying contributing analyses, the best architectures, based purely on performance, are either a pump-fed NTO/MMH lander or a LOX/LH_2 RBO lander; both systems will perform well with existing engines. Finally, because of the 2024 target date for the first crewed landing, it is unlikely that a RBO CFM system would be mature such that it could fly on a man-rated lunar lander; this analysis has shown that a passive CFM lander can be used for initial landings and eventually evolved into lander with an RBO CFM system. While these concepts are promising, further analysis is warranted to understand the campaign-level impacts of decent stage trades on the overall Artemis landing system as well as the ability to meet the 2024 target date.

9. Acknowledgments

We would like to thank Stephen Edwards and Doug Trent for their work on DYREQT and for their input into this work. We would also like to thank D.R. Komar for providing insight into spacecraft power systems.

References

[1] National Aeronautics and Space Administration. Commercial Lunar Payload Services (CLPS) Solicitation 80HQTR18R0011R, 2018.

[2] Chang, Kenneth. NASA Hires 3 Companies for Moon Science Deliveries. *New York Times*, May 2019.

[3] Crusan, Jason. Gateway update, December 2018. Presentation to NASA Advisory Council.

[4] K. Deb, A. Pratap, S. Agarwal, and T. Meyarivan. A fast and elitist multiobjective genetic algorithm: NSGA-II. *IEEE Transactions on Evolutionary Computation*, 6(2):182–197, apr 2002.

[5] Edwards, Stephen J. *A Methodology for Risk-Informed Launch Vehicle Architecture Selection*. PhD thesis, Georgia Institute of Technology, 2017.

[6] Edwards, Stephen J., Manuel J. Diaz, Dimitri N. Mavris, and Douglas Trent. A Model-Based Framework for Synthesis of Space Transportation Architectures. In *2018 AIAA SPACE and Astronautics Forum and Exposition*. American Institute of Aeronautics and Astronautics, sep 2018.

[7] Fesmire, J. E., B. E. Coffman, B. J. Meneghelli, and K. W. Heckle. Spray-on foam insulations for launch vehicle cryogenic tanks. *Cryogenics*, 52(4-6):251–261, 2012.

[8] Gray, Justin, Kenneth Moore, Tristan Hearn, and Bret Naylor. A Standard Platform for Testing and Comparison of MDAO Architectures. In *53rd AIAA/ASME/ASCE/AHS/ASC Structures, Structural Dynamics and Materials Conference*. American Institute of Aeronautics and Astronautics, 2012.

[9] Gray, Justin S., John T. Hwang, Joaquim R. R. A. Martins, Kenneth T. Moore, and Bret A. Naylor. OpenMDAO: An Open-Source Framework for Multidisciplinary Design, Analysis, and Optimization. *Structural and Multidisciplinary Optimization*, 59(4):1075–1104, 2019.

[10] Kos, Larry. Personal Communication.

[11] Kos, Larry, Tara Polsgrove, Ronald Sostaric, Ellen Braden, Jacob Sullivan, and Thanh Le. Altair Descent and Ascent Reference Trajectory Design and Initial Dispersion Analyses. In *AIAA Guidance, Navigation, and Control Conference*, 2010.

[12] Mendez Ramos, Eugina D., Manuel J. Diaz, Bradford Robertson, and Dimitri Mavris. Development of a Physics-Based Reusable Cargo Lunar Lander Modeling and Simulation Capability. In *70th International Astronautical Congress*, Washington D. C., October 2019.

[13] National Aeronautics and Space Administration. NASA Expands Plans for Moon Exploration: More Missions, More Science, May 2018.

[14] National Aeronautics and Space Administration. NASA Outlines New Lunar Science, Human Exploration Missions, March 2019.

[15] National Aeronautics and Space Administration. NASA Taps 11 American Companies to Advance Human Lunar Landers, May 2019.

[16] National Aeronautics and Space Administration. Next Space Technologies for Exploration Partnerships - 2 Appendix E: Human Landing System Studies, Risk Reduction, Development, and Demonstration Broad Agency Announcement NNH19ZCQ001K Appendix E, February 2019.

[17] Plachta, David W., R. J. Christie, E. Carlberg, and J. R. Feller. Cryogenic propellant boil-off reduction system. In *AIP Conference Proceedings*, volume 985, pages 1457–1466. AIP, 2008.

[18] Sudol, Alicia, Stephen J. Edwards, and Dimitri N. Mavris. Technology assessment for launch vehicle concepts using the DYnamic rocket equation tool (DYREQT). In *2018 AIAA SPACE and Astronautics Forum and Exposition*. American Institute of Aeronautics and Astronautics, sep 2018.

[19] Sutherlin, Steven and Wesley Johnson. *Cryogen Storage Integrated Model (CryoSIM) Version 3*. NASA Marshall Space Flight Center, October 2014.

[20] Trent, Douglas and Dimitri N. Mavris. Impacts on High-level Systems-of-Systems Figures of Merit due to Integrated Architecture Sizing and Technology Evaluation at the Subsystem-Level. In *2018 AIAA SPACE and Astronautics Forum and Exposition*. American Institute of Aeronautics and Astronautics, sep 2018.

[21] Trent, Douglas J. *Integrated Architecture Analysis and Technology Evaluation for System of Systems Modeled at the Subsystem Level*. PhD thesis, Georgia Institute of Technology, 2017.

[22] Wertz, J. R., David F. Everett, and Jeffery J. Pushcell. *Space Mission Engineering: The New SMAD*. Microcosm Press, 2011.

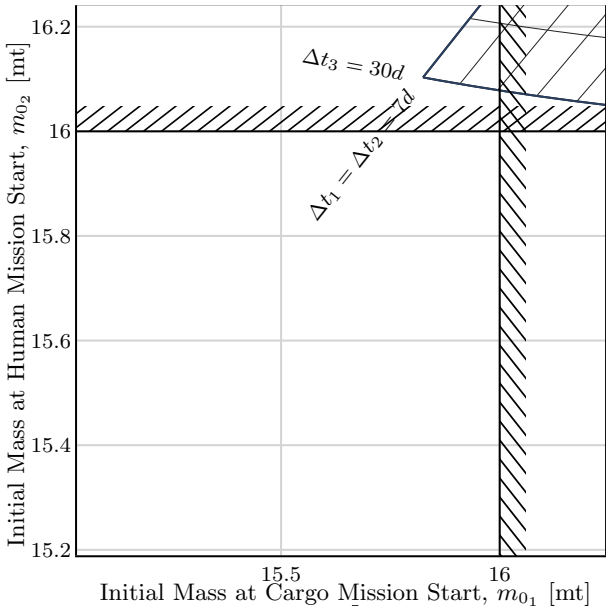

(a) 2 Fuel & 2 Ox Tanks

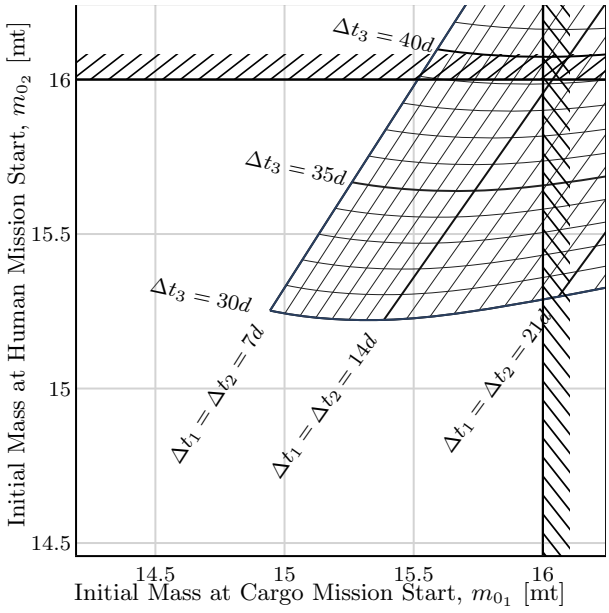

(b) 1 Fuel & 4 Ox Tanks

Fig. 7: A close view of the feasible portion of the envelope for Passive LH_2 architectures with fast transit to Gateway

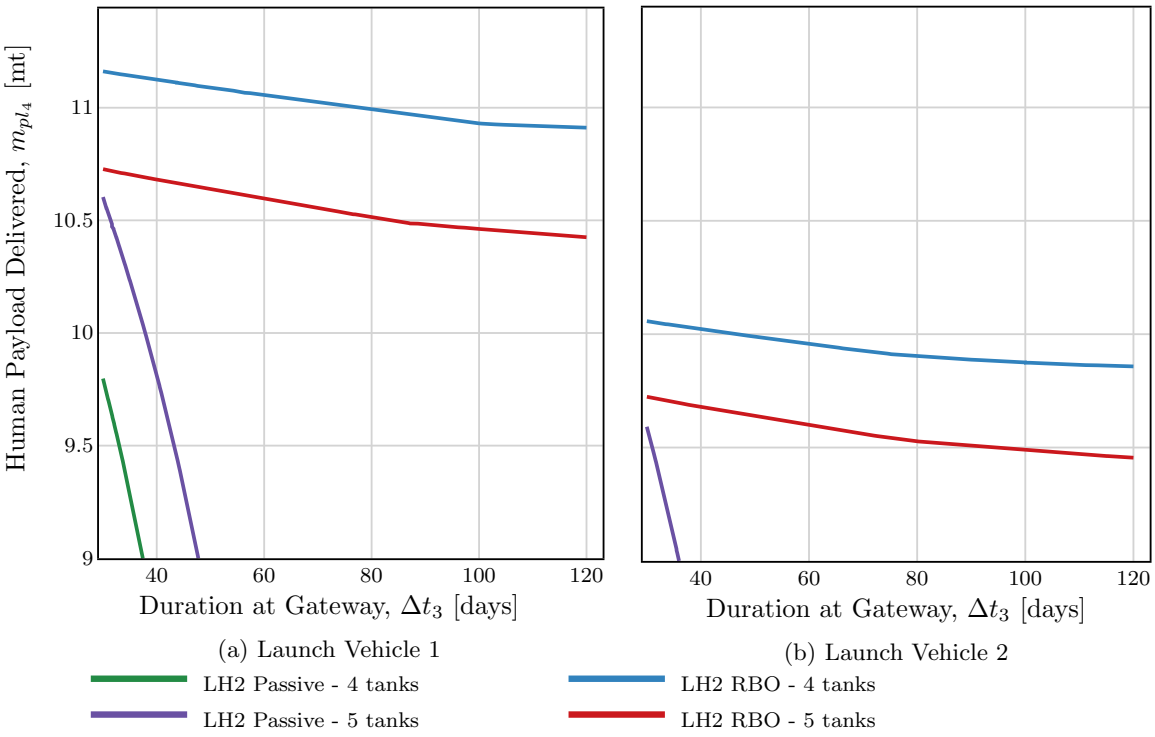

Fig. 8: A comparison of LH_2 Architectures 4 vs 5 Tanks on fast Gateway transit option

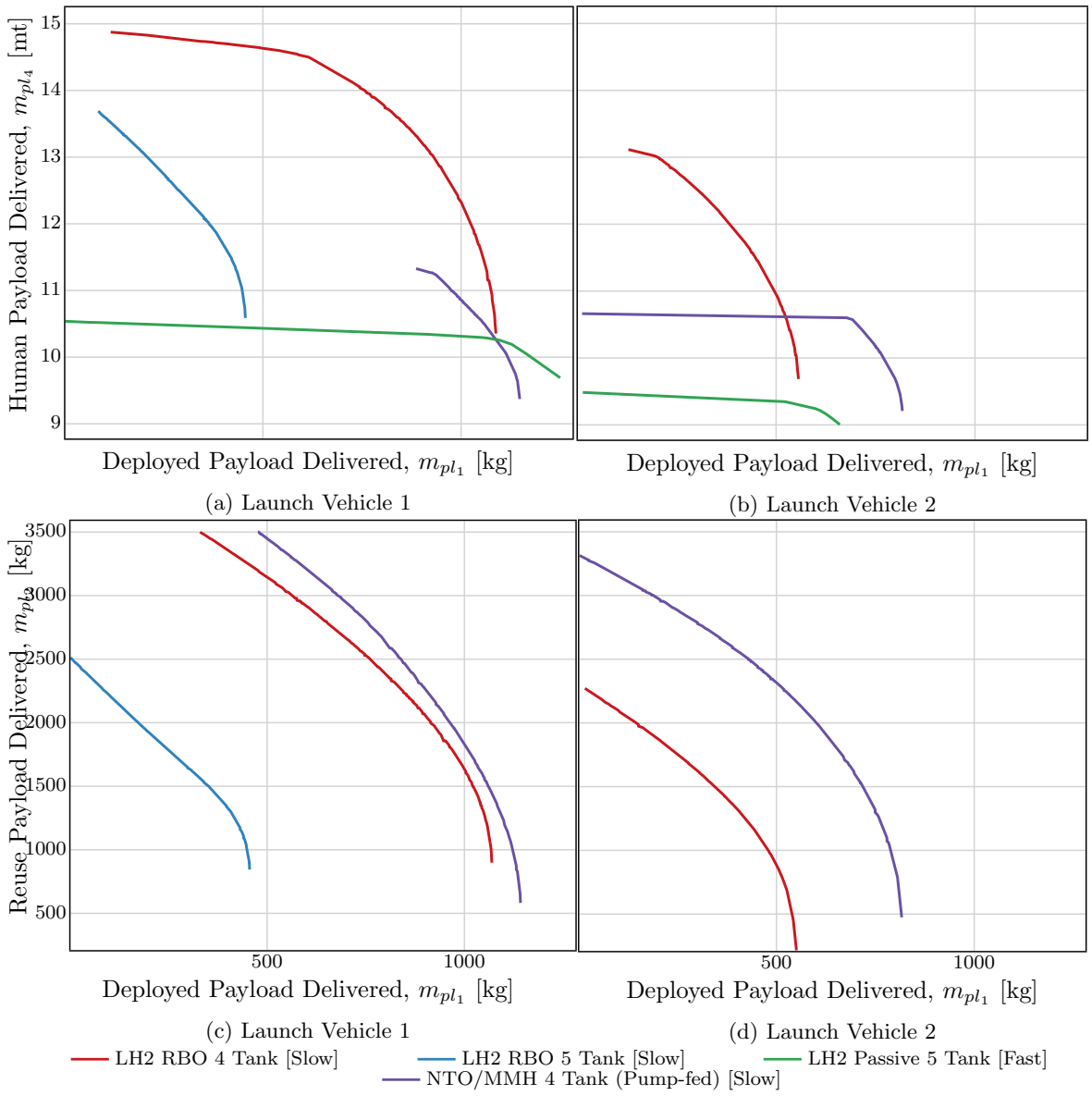

Fig. 9: Constrained Pareto Frontiers showing architectures utilizing COTS engines